

# DiMoDif: Discourse Modality-information Differentiation for Audio-visual Deepfake Detection and Localization

Christos Koutlis, Symeon Papadopoulos  
Information Technologies Institute @ CERTH  
Thessaloniki, Greece  
{ckoutlis,papadop}@iti.gr

## Abstract

Deepfake technology has rapidly advanced, posing significant threats to information integrity and societal trust. While significant progress has been made in detecting deepfakes, the simultaneous manipulation of audio and visual modalities, sometimes at small parts but still altering the meaning, presents a more challenging detection scenario. We present a novel audio-visual deepfake detection framework that leverages the inter-modality differences in machine perception of speech, based on the assumption that in real samples – in contrast to deepfakes – visual and audio signals coincide in terms of information. Our framework leverages features from deep networks that specialize in video and audio speech recognition to spot frame-level cross-modal incongruities, and in that way to temporally localize the deepfake forgery. To this end, DiMoDif employs a Transformer encoder-based architecture with a feature pyramid scheme and local attention, and optimizes the detection model through a composite loss function accounting for frame-level detections and fake intervals localization. DiMoDif outperforms the state-of-the-art on the Temporal Forgery Localization task by +47.88% AP@0.75 on AV-Deepfake1M, and performs on-par on LAV-DF. On the Deepfake Detection task, it outperforms the state-of-the-art by +30.5% AUC on AV-Deepfake1M, +2.8% AUC on FakeAVCeleb, and performs on-par on LAV-DF. Code available at <https://github.com/mever-team/dimodif>.

## 1 Introduction

Audio-visual deepfakes are AI-generated content involving manipulations to one or both modalities, sometimes at small time intervals, with the intention to deceive [45]. Deepfake content can widely spread online, and mislead viewers, contributing to the growing issue of information disorder. A common feature of audio-visual deepfakes is the presence of incongruities between the visual and audio signals, which are, however, increasingly hard to detect manually. This necessitates the development of robust AI-based deepfake detection methods.

Deepfake detection is a growing area of research

[54, 51, 46]. Existing approaches primarily focus on pixel-level analysis, which examines inconsistencies in gradient variations [65], color variations [30], or artifacts introduced during the generation process [11]. Also, feature-based methods analyze facial landmarks [72], temporal coherence [27], and other visual cues to identify inconsistencies in deepfake content [40]. Furthermore, there has been growing interest in detecting and localizing deepfakes in audio-visual content, with both tasks being particularly challenging due to the complex interplay between the two modalities. Key approaches include audio-visual synchronization that analyzes the consistency between visual and auditory cues namely face movements and speech [26, 9, 14], feature reconstruction learning with cross-reconstruction similarity estimation to detect anomalies prevalent in fake videos [76], and self-supervised approaches relying on the synchronization patterns learned from real videos only [28, 18].

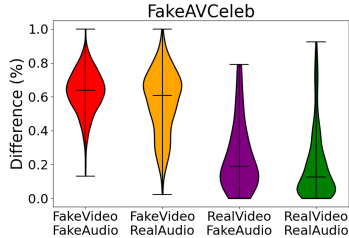
Humans integrate multimodal sensory information, such as visual and auditory input, to extract meaningful features and perform a wide range of recognition tasks. Cognitive neuroscience research has extensively documented the interplay between video and audio [63, 64], often resulting in the alteration of perceptual content [70, 13] or even the induction of perceptual illusions [52, 60]. In the context of speech perception, the brain actively constructs content representations by combining visual, auditory, and contextual cues to predict ongoing and future utterances [12]. When visual information conflicts with auditory input, as in the McGurk effect [49] or in the case of deepfakes, increased prediction errors are observed, accompanied by significant changes in brain activity, which often manifest as higher-frequency neural oscillations and localized activation patterns, indicative of heightened cognitive effort [4].

We illustrate how state-of-the-art AI analysis tools could emulate this process in Figure 1. In Figure 1a, an input video is first decomposed into its constituent visual and audio streams. These are then fed into state-of-the-art models for lip-reading and speech-recognition [44], and the resulting textual outputs are compared<sup>1</sup>. Their difference is computed using the

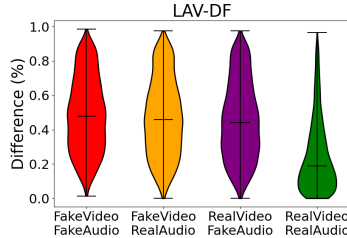
<sup>1</sup>Python’s `diff`lib is used (cf. <https://docs.python.org/3/library/difflib.html>).



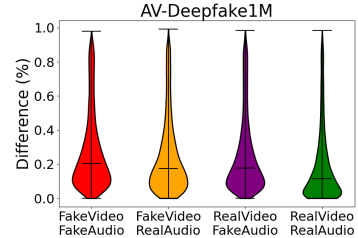
(a) Example of speech recognition differences between lip-reading and speech-to-text models.



(b) Aggr. FakeAVCeleb [34].



(c) Aggr. LAV-DF [10].



(d) Aggr. AV-Deepfake1M [8].

Figure 1: The process of identifying audio-visual inconsistency for deepfake detection. In (a), a video’s visual and audio components are separately processed by lip-reading and speech-to-text models, then a difference score is calculated. In (b,c,d) the difference score distributions are illustrated in the form of violin plots for three different datasets.

normalized Levenshtein distance, i.e. the ratio between the edit distance  $\delta$  of the two sentences and the sum of their lengths, which results in scores between 0% (identical) and 100% (completely different). Figures 1b to 1d illustrate aggregate results through violin plots computed on the evaluation sets of three popular audio-visual deepfake detection benchmarks, FakeAVCeleb [34], LAV-DF [10], and AV-Deepfake1M [8]. On average, lower difference is observed in real videos compared to fake ones across all datasets, indicating the suitability of this score as a measure of incongruity between audio and video. Even though these differences are significant on FakeAVCeleb, they are smaller on LAV-DF, and much smaller on AV-Deepfake1M, which render naive thresholding on this score unsuitable for robust detection. This is due to the fact that FakeAVCeleb’s videos are fully manipulated, while LAV-DF’s samples are manipulated only in parts, while samples from AV-Deepfake1M are manipulated in even smaller parts (on average half the length of those in LAV-DF).

Motivated by the above, we propose Discourse Modality-information Differentiation (DiMoDif), a deep learning-based deepfake detection architecture that exploits the inter-modality differences in machine perception of speech. DiMoDif first decomposes the input video into its visual and audio streams, and extracts the respective video and audio representations based on state-of-the-art lip reading and speech-to-text pre-trained models [44]. At its core, DiMoDif employs a Transformer encoder architecture [66] with a feature pyramid scheme and local attention configuration, to spot frame-level cross-modal incongruities between the two modality-specific representations, and

in that way detect and localize the deepfake forgeries. Note that low difference scores frequently occur in partly manipulated fake videos (e.g. Figure 1a); however, DiMoDif manages to classify them as fake by capturing audio-visual divergence at the frame level. In addition, high difference scores occasionally occur in real videos; however, DiMoDif leverages alternative features, e.g., hard *phonemes* [6], to classify them as real (cf. Section 5.2). The architecture is optimized using a composite loss function that accounts for frame-specific detections, overlaps between predicted and ground truth fake intervals, and divergence in corresponding boundaries. We evaluate DiMoDif on Deepfake detection (DFD) and Temporal Forgery Localization (TFL) tasks using three audio-visual deepfake detection benchmarks, FakeAVCeleb [34], LAV-DF [10], and AV-Deepfake1M [8]. DiMoDif outperforms the state-of-the-art on FakeAVCeleb by +2.8% AUC, exhibits a significant performance increase of +30.5% AUC and +47.88% AP@0.75 on AV-Deepfake1M, and performs on-par on LAV-DF dataset. We also provide an analysis of DiMoDif’s generalization abilities, and an extensive ablation analysis to ground our methodological choices.

## 2 Related Work

### 2.1 Deepfake Detection Datasets

During the past years, several datasets have been proposed for video deepfake detection. Most of them focus solely on visual manipulations, thus including only the visual modality in their samples, e.g.,

dataset	size	content		manip.		target			task
		A	V	A	V	A	V	joint	
DFDC [20]	128,154	✓	✓	✓	✓	✗	✗	✓	DFD
KoDF [36]	237,942	✓	✓	✗	✓	✗	✓	✗	DFD
FakeAVCeleb [34]	21,544	✓	✓	✓	✓	✓	✓	✗	DFD
LAV-DF [10]	136,304	✓	✓	✓	✓	✓	✓	✗	DFD,TFL
AV-Deepfake1M [8]	1,146,760	✓	✓	✓	✓	✓	✓	✗	DFD,TFL

Table 1: Deepfake detection datasets providing both video and audio. Size determines the number of samples, content specifies the provided modalities, manipulation specifies which modality has been manipulated, target specifies for which modality the dataset provides ground truth, while task is reported in the last column.

DF-TIMIT [35], FaceForensics++ [58], DeeperForensics [32], Celeb-DF [41], WildDeepfake [81], and DF-Platter [48]. Our focus is on the detection of audio-visual deepfakes, which require content, manipulations and annotations in both modalities. Table 1 presents deepfake detection datasets that provide both visual and audio streams. DFDC [20] is a seminal large-scale benchmark in the field that contains approximately 128K samples. Although it provides audio-visual content and contains manipulations on both modalities, (i) it does not provide separate manipulation annotations per modality, (ii) fake audio parts appear in only 4% of the total number of videos, while fake visual parts in 84%<sup>2</sup>, and (iii) it contains videos where the depicted individual does not talk or the speaking person is not depicted and the depicted one does not talk. These features render DFDC inappropriate for audio-visual deepfake detection. KoDF [36] is another large-scale benchmark containing 237K videos of Korean subjects. Although it provides both the visual and audio components of its samples, it contains only visual manipulations, which makes it unsuitable for our problem. FakeAVCeleb [34], contains 21K manipulated and 0.5K real videos with manipulations on both modalities and corresponding annotations. Due to its size it is commonly used as an evaluation benchmark; here, we consider it for training and evaluation purposes with real video additions from the VoxCeleb2 dataset [15]. LAV-DF [10] is a recently introduced dataset that contains 136K real and fake videos with manipulations and targets on both modalities for two tasks, Deepfake Detection (DFD) and Temporal Forgery Localization (TFL). Finally, AV-Deepfake1M [8] is the largest audio-visual deepfake detection benchmark to date containing over 1.1M real and fake videos with manipulations and targets on both modalities, for both the DFD and TFL tasks. In our experimental analysis, we consider FakeAVCeleb, LAV-DF, and AV-Deepfake1M datasets, which meet all requirements of the audio-visual deepfake detection task. We also consider DFDC and KoDF for cross-dataset generalization evaluation experiments.

<sup>2</sup>Based on a later estimation: <https://www.kaggle.com/datasets/basharallabadi/dfdc-video-audio-labels>.

## 2.2 Deepfake Detection Approaches

Many deepfake detection approaches consider only video-level manipulations and processing [62, 58, 78, 38, 1, 17, 55]. Although these are only partly related to DiMoDif we compare our method with them following previous practice. Recent works in deepfake detection have focused on leveraging both visual and audio information through learning mechanisms based on multimodal fusion, contrastive learning, and self-supervised-learning, aiming to uncover cross-modal inconsistencies in deepfake videos. Specifically, [80] demonstrated the effectiveness of an attention-based detection framework that identifies the violation of cross-modal synchronization patterns in deepfake videos, while [71] proposed a framework exploiting audio-visual inconsistency by encoding spatio-temporal information, fusing multimodal features, and then classifying based on inter- and intra-modal disharmony levels. Similarly, [56, 31, 82] propose joint representation learning frameworks that consider inter- and intra-modal encoding mechanisms. UMMAFormer [76] adopts feature reconstruction and cross-reconstruction attention combined with an enhanced feature pyramid network, while BA-TFD & BA-TFD+ [10, 9] adopt 3DCNN and multi-scale vision Transformer backbones guided by contrastive, frame classification, and boundary matching objectives. The contrastive learning approach is also adopted by other works for comparing inter-modal representations within a video [14] or between different videos [77]. Other papers focus on feature similarity to identify audio-visual inconsistencies [26], and [59] compares features of the video’s lip sequence with a lip sequence generated from the audio input. Self-supervised approaches that leverage intrinsic synchronization of real videos have also been utilized [75, 25, 28, 22, 18, 53, 73, 21] to tackle the generalization challenge faced by methods trained on specific deepfake generation models. A similar motivation with ours is presented in [7, 39], which rely on a simple threshold on the divergence between visual and audio speech recognition model outputs. However, as shown in Figure 1 this simple technique is insufficient on benchmarks with harder samples than FakeAVCeleb, such as LAV-DF and AV-Deepfake1M. In contrast, our approach extracts lip-reading and speech-to-text content representations that are then processed by a Transformer-based fusion mechanism that is capable of identifying discriminative speech features on top of speech divergence ones. Pre-trained lip-reading models have also been utilized as feature extractors in [29], but for visual-only deepfake detection. In addition, [57] sets a threshold on cross-modal feature similarity deriving from an audio-visual speech self-supervised representation learning model. Also, specialized representation learning has been explored by [47] that considers modality emotion consistency and [69] that considers articulatory and lip movement consistency. Finally, several works [42, 50, 61, 74, 5] of the Temporal Action Localization (TAL) domain are considered

as relevant by the deepfake detection literature.

### 3 Methodology

#### 3.1 Problem Formulation

Consider a dataset  $\mathcal{D} = \{\mathbf{v}_i, y_i, \mathbf{y}_i\}_{i=1}^N$  where  $\mathbf{v}_i = \{v, a\}$  denotes a video, containing the visual  $v \in \mathbb{R}^{h \times w \times c \times f}$  and the audio  $a \in \mathbb{R}^s$  signal<sup>3</sup>, with  $h$  denoting the height,  $w$  the width,  $c$  the number of channels,  $f$  the number of video frames, and  $s$  the number of audio samples.  $y_i \in \{0, 1\}^2$  denotes the Deepfake Detection (DFD) target per modality, while  $\mathbf{y}_i = \{y_{i,1}^v, \dots, y_{i,f}^v, y_{i,1}^a, \dots, y_{i,f}^a\}$ , with  $y_{i,j}^m = (d_{i,j}^{m,s}, d_{i,j}^{m,e}, a_{i,j}^m)$ , denotes the Temporal Forgery Localization (TFL) target, assigning a forgery ground truth  $a_{i,j}^m \in \{0, 1\}$  to each modality  $m \in \{v, a\}$  and frame  $j$ , along with the corresponding distances  $d_{i,j}^{m,s}, d_{i,j}^{m,e} \in \mathbb{R}$  between the frame  $j$  and the onset  $s_{i,j}^m$  and offset  $e_{i,j}^m$  of the fake interval, if the frame  $j$  is fake. We train deep networks  $\mathcal{F}$ , the architecture of which is analysed in Section 3.2, on the DFD task  $\hat{y}_i = \mathcal{F}(\mathbf{v}_i)$  and the TFL task  $\hat{\mathbf{y}}_i = \mathcal{F}(\mathbf{v}_i)$  separately, while the predictions  $\hat{\mathbf{y}}_i$  are decoded by:

$$\hat{a}_{i,j}^m > 0.5, \hat{s}_{i,j}^m = j - \hat{d}_{i,j}^{m,s}, \hat{e}_{i,j}^m = j - \hat{d}_{i,j}^{m,e} \quad (1)$$

$\hat{\cdot}$  denotes prediction while its absence ground truth. Henceforth, we omit sample index  $i$  to reduce notation complexity.

#### 3.2 Architecture

Our architecture is illustrated in Figure 2. From each video  $\mathbf{v} = \{v, a\}$ , we extract the visual  $\mathbf{v} \in \mathbb{R}^{f \times d_0}$  and audio  $\mathbf{a} \in \mathbb{R}^{f \times d_0}$  features corresponding to its visual  $v$  and audio  $a$  components, denoting with  $d_0$  the embedding dimension, based on the lip-reading and speech-to-text models proposed in [44]. Under ideal conditions, in real videos,  $\mathbf{v}$  and  $\mathbf{a}$  contain the same information corresponding to the discourse, while in deepfakes that contain manipulated parts, differentiation is expected. For that reason, the proposed architecture that identifies such patterns is named Discourse Modality-information Differentiation (DiMoDif).

The discourse features,  $\mathbf{v}$  and  $\mathbf{a}$ , are projected to  $d$  dimensions using a lightweight 1-D convolutional network with two ReLU-activated layers. Then, we add trainable sequence encoding  $S_v, S_a \in \mathbb{R}^d$  and employ a separation token  $\mathbf{s} \in \mathbb{R}^d$  to encode modality information. An additional classification token  $\mathbf{c} \in \mathbb{R}^d$  is only employed in DFD experiments, and position encoding  $P_j \in \mathbb{R}^d$ , with  $j = 1, \dots, 2 \cdot f + e$ , is applied on all tokens, resulting in tensor  $\mathbf{t} = \oplus\{\mathbf{c}, \mathbf{v}, \mathbf{s}, \mathbf{a}\} \in \mathbb{R}^{(2 \cdot f + e) \times d}$ , with  $\oplus$  denoting concatenation, being the input to the Transformer encoder  $\mathcal{T}$  [66].  $e$  depends on the task, being equal to 2 in DFD experiments and equal to 1 in TFL experiments where  $\mathbf{c}$  is absent.

<sup>3</sup>Utterances mainly comprise monophonic signals, besides conversion to single-channel is straightforward if required.

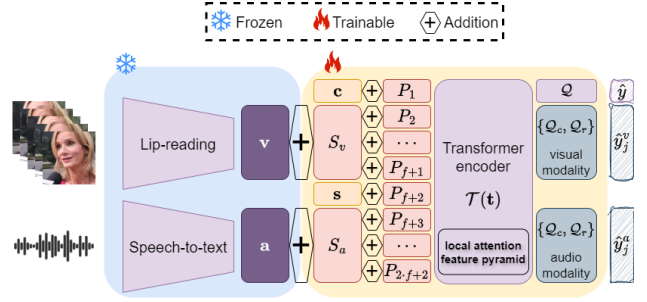


Figure 2: The DiMoDif architecture.

Then, we extract  $d$ -dimensional feature pyramids corresponding to all  $2 \cdot f$  visual and audio tokens deriving from all  $l$  layers of the Transformer encoder, denoted by  $\mathbb{R}^{(2 \cdot f) \times l \times d} \ni \mathbf{z} \subset \mathcal{T}(\mathbf{t})$ . To do so,  $\mathcal{T}$  processes  $\mathbf{t}$  as:

$$\tilde{\mathbf{z}}_j = \text{MSA}(\text{LN}(\mathbf{z}_{j-1})) \quad (2)$$

$$\mathbf{z}_j = \text{MLP}(\text{LN}(\tilde{\mathbf{z}}_j)) + \tilde{\mathbf{z}}_j \quad (3)$$

where  $j = 1, \dots, l$  denotes the layer index,  $\mathbf{z}_0 = \mathbf{t}$  is the input, MSA denotes Multi-head Softmax Attention [66] with  $r$  number of heads, LN denotes Layer Normalization [37], and MLP denotes a Multi-Layer Perceptron with internal dimensionality  $d \cdot u$ . Then,  $\mathbf{z} = \oplus\{\mathbf{z}_j\}_{j=1}^l$ , omitting the tokens that correspond to  $\mathbf{c}$  and  $\mathbf{s}$ . Given that short-term inter-modality inconsistency detection is key to our tasks, local attention is preferable in contrast to global; besides, it is computationally more efficient. Thus, we limit the Transformer's attention to a local window  $[j - q/2, j + q/2]$  of  $q$  tokens around each token  $j$ .

Finally, in DFD experiments, predictions  $\hat{y}$  are made by a feed-forward classification head  $\mathcal{Q}$  that takes as input the classification tokens of  $\mathbf{z}$ , denoted by  $\mathbf{z}' \in \mathbb{R}^{l \times d}$ , and consists of three linear layers, the first two of which are followed by Layer Normalization (LN) and ReLU activation:

$$\mathbf{z}'' = \text{ReLU}(\text{LN}(\mathbf{z}' \cdot \mathbf{W}_1 + \mathbf{b}_1)) \quad (4)$$

$$\mathbf{z}''' = \text{ReLU}(\text{LN}(\mathbf{z}'' \cdot \mathbf{W}_2 + \mathbf{b}_2)) \quad (5)$$

$$\hat{y} = \mathbf{z}''' \cdot \mathbf{W}_3 + \mathbf{b}_3 \quad (6)$$

where  $\mathbf{W}_1, \mathbf{W}_2 \in \mathbb{R}^{d \times d}$ ,  $\mathbf{b}_1, \mathbf{b}_2 \in \mathbb{R}^d$ ,  $\mathbf{W}_3 \in \mathbb{R}^{d \times 2}$ ,  $\mathbf{b}_3 \in \mathbb{R}^2$  are learnable parameters, and  $\hat{y} \in \mathbb{R}^{l \times 2}$  are the logits for the video and audio modalities per Transformer layer. In TFL experiments, predictions  $\hat{\mathbf{y}}$  are made by two lightweight 1-D convolutional networks, namely the classification  $\mathcal{Q}_c$  and regression  $\mathcal{Q}_r$  heads, each consisting of three convolutional layers, the first two of which are followed by Layer Normalization (LN) and ReLU activation. The classification head predicts  $l$  probabilities  $\hat{a}_j^m \in \mathbb{R}^l$  for frame  $j$  of modality  $m$  to be fake, while the regression head predicts  $l$  distance pairs  $(\hat{d}_j^{m,s}, \hat{d}_j^{m,e}) \in \mathbb{R}^{l \times 2}$ , respectively.

#### 3.3 Objective Function

For the DFD task, we consider the binary cross-entropy loss [24], directly optimizing the real vs. fake

objective. For the TFL task, we propose a composite loss as the combination of three loss functions, namely (1) the focal loss [43] to optimize the classification objective, while accounting for class imbalance being prevalent in each video’s frames, (2) the DIOU loss [79] to optimize the regression objective by maximizing the overlap between predicted and ground truth fake time intervals, and (3) the smooth L1 loss [23] to minimize the distance between predicted and actual boundaries of fake time intervals. Detailed mathematical expressions explaining the computation of both loss functions can be found in the Appendix A.

## 4 Experimental Setup

### 4.1 Datasets

We consider FakeAVCeleb [34], LAV-DF [10], and AV-Deepfake1M [8] datasets for training and evaluation. Appendix B provides details on class and split sizes. FakeAVCeleb contains 21K fake and 500 real samples, thus for balance we added 20K more from VoxCeleb2 dataset [15] including 10K of male and 10K of female speakers of several ethnicities talking in English<sup>4</sup>, reaching a total of 41,544 samples randomly split based on a 80-10-10 identity separation. LAV-DF has been released with standard splits of 78K training, 31K validation, and 26K test samples. AV-Deepfake1M has 746K training, 57K validation, and 343K test samples the metadata of which have not been released. We also evaluate DiMoDif on the test set of DFDC [20] and a randomly selected 6K-sized sample from KoDF [36] proportionally spanning all synthesis methods and real samples, to assess generalization.

### 4.2 Evaluation

For DFD, we use accuracy (ACC), Average Precision (AP), and area under ROC curve (AUC). For TFL, we use Average Precision at  $p$  (AP@ $p$ ), and Average Recall at  $n$  (AR@ $n$ ). We report metrics per dataset in accordance to previous works for comparability. On AV-Deepfake1M we evaluate through Codabench<sup>5</sup>. Competing methods are audio-visual deepfake detectors, face manipulation detectors, and temporal action localization models, discussed in Section 2.

### 4.3 Implementation Details

We train DiMoDif for 100 epochs with early stopping patience 10 and checkpoint based on validation metrics, AUC for DFD and the sum of AP@ $p$  and AR@ $n$  for TFL. Batch size is set to 64, initial learning rate to 0.001 with ReduceLRonPlateau scheduler<sup>6</sup> and Adam optimizer, local attention

window size  $q$  to 15, and focal loss’ hyperparameters  $\alpha = 0.98$  and  $\gamma = 2$ . Also, we set a maximum sequence length  $f$  to 600 and zero-pad the smaller. We consider a grid for  $\mathcal{T}$ ’s size, with  $(d, r, u) \in \{(32, 2, 1), (64, 2, 1), (64, 4, 1), (128, 4, 2), (256, 8, 2)\}$  and number of layers  $l \in \{1, 3, 5\}$ . Grid search for AV-Deepfake1M is performed with 200K training samples to reduce resource requirements, but retrain the best configuration on the whole set. We spent  $\sim 3900$  GPU hours for training on NVIDIA GeForce RTX 3090 Ti GPUs.

## 5 Results

### 5.1 Temporal Forgery Localization

Tables 2 and 3 present the performance of our method in comparison to state-of-the-art, in terms of Temporal Forgery Localization (TFL), on LAV-DF [10] and AV-Deepfake1M [8] datasets, respectively. On LAV-DF, DiMoDif outperforms all competitive approaches wrt AR@{100,50,20}, is second to best wrt AR@10, and third wrt AP@{0.5,0.75,0.95}. UMMAFormer [76], BA-TFD+ [9] and ActionFormer [74] exhibit similar performance, while the rest of the models have lower localization abilities. On AV-Deepfake1M, DiMoDif outperforms all competitive approaches wrt all metrics exhibiting significant performance increase. The proposed method’s AR is almost double compared with the second to best, while it exhibits a notable absolute increase of +35.29% and +47.88% in AP at 0.5 and 0.75, respectively.

### 5.2 Deepfake Detection

Tables 4 to 6, present comparative results in terms of video-level Deepfake Detection (DFD) on LAV-DF [10], AV-Deepfake1M [8], and FakeAVCeleb [34], respectively. On LAV-DF, DiMoDif performs on-par with the state-of-the-art method UMMAFormer [76], achieving 99.6 AUC, better than the remaining competitive methods. On AV-Deepfake1M dataset, DiMoDif outperforms all state-of-the-art competitive methods by a significant absolute performance increase of +30.5% in terms of AUC<sup>7</sup>. On FakeAVCeleb, DiMoDif outperforms all competitive methods on average achieving +4.1% absolute AP increase, and +2.8% absolute AUC increase, as well as in most forgery types. Finally, challenging real samples with normalized Levenshtein distance over 0.8 (cf. Section 1), are scored by DiMoDif with an average of 0.19, and 0.16 on LAV-DF, and AV-Deepfake1M, respectively, attesting to DiMoDif’s advantage wrt a naive distance-thresholding approach.

<sup>4</sup>Language identification conducted with <https://github.com/speechbrain/speechbrain>.

<sup>5</sup><https://deepfakes1m.github.io/evaluation>

<sup>6</sup>[https://pytorch.org/docs/stable/generated/torch.optim.lr\\_scheduler.ReduceLRonPlateau.html](https://pytorch.org/docs/stable/generated/torch.optim.lr_scheduler.ReduceLRonPlateau.html)

<sup>7</sup>Accuracy (ACC) is also reported by other papers; however, Codabench does not provide it for the test samples, thus we report the validation accuracy, which, even though is not comparable, still provides a sense on the level of uncalibrated threshold performance increase.

Method	Modality	AP@0.5	AP@0.75	AP@0.95	AR@100	AR@50	AR@20	AR@10
MDS [14]	$\mathcal{AV}$	12.8	1.6	0.0	37.9	36.7	34.4	32.2
AGT [50]	$\mathcal{V}$	17.9	9.4	0.1	43.2	34.2	24.6	16.7
BMN [42]	$\mathcal{V}$	24.0	7.6	0.1	53.3	41.2	31.6	26.9
BMN (I3D) [42]	$\mathcal{V}$	10.6	1.7	0.0	48.5	44.4	37.1	31.6
AVFusion [5]	$\mathcal{AV}$	65.4	23.9	0.1	63.0	59.3	54.8	52.1
ActionFormer [74]	$\mathcal{V}$	95.3	<u>90.2</u>	<u>23.7</u>	88.4	89.6	90.3	90.4
BA-TFD [10]	$\mathcal{AV}$	76.9	38.5	0.3	66.9	64.1	60.8	58.4
BA-TFD+ [9]	$\mathcal{AV}$	<u>96.3</u>	85.0	4.4	81.6	80.5	79.4	78.8
UMMAFormer [76]	$\mathcal{AV}$	<b>98.8</b>	<b>95.5</b>	<b>37.6</b>	<u>92.4</u>	<u>92.5</u>	<u>92.5</u>	<b>92.1</b>
DiMoDif (ours)	$\mathcal{AV}$	95.5	87.9	20.6	<b>94.2</b>	<b>93.7</b>	<b>92.7</b>	<u>91.4</u>

Table 2: Temporal forgery localization results on LAV-DF [10]. Modality denotes the model’s input type with  $\mathcal{V}$  being visual and  $\mathcal{A}$  audio. **Bold** indicates best and underline second to best performance.

Method	Modality	AP@0.5	AP@0.75	AP@0.9	AP@0.95	AR@50	AR@30	AR@20	AR@10	AR@5
Meso4 [1]	$\mathcal{V}$	09.86	06.05	02.22	00.59	38.92	38.91	38.81	36.47	26.91
MesoInception4 [1]	$\mathcal{V}$	08.50	05.16	01.89	00.50	39.27	39.22	39.00	35.78	24.59
EfficientViT [17]	$\mathcal{V}$	14.71	02.42	00.13	00.01	27.04	26.99	26.43	23.90	20.31
TriDet+VideoMAEv2 [61, 67]	$\mathcal{V}$	21.67	05.83	00.54	00.06	20.27	20.23	20.12	19.50	18.18
TriDet+InternVideo [61, 68]	$\mathcal{V}$	29.66	09.02	00.79	00.09	24.08	24.06	23.96	23.50	22.55
ActionFormer+VideoMAEv2 [74, 67]	$\mathcal{V}$	20.24	05.73	00.57	00.07	19.97	19.93	19.81	19.11	17.80
ActionFormer+InternVideo [74, 68]	$\mathcal{V}$	36.08	12.01	01.23	00.16	27.11	27.08	27.00	26.60	25.80
BA-TFD [10]	$\mathcal{AV}$	37.37	6.34	0.19	0.02	45.55	40.37	35.95	30.66	26.82
BA-TFD+ [9]	$\mathcal{AV}$	44.42	13.64	0.48	0.03	<u>48.86</u>	<u>44.51</u>	40.37	34.67	29.88
UMMAFormer [76]	$\mathcal{AV}$	<u>51.64</u>	<u>28.07</u>	<u>7.65</u>	<u>1.58</u>	44.07	43.93	<u>43.45</u>	<u>42.09</u>	<u>40.27</u>
DiMoDif (ours)	$\mathcal{AV}$	<b>86.93</b>	<b>75.95</b>	<b>28.72</b>	<b>5.43</b>	<b>81.57</b>	<b>80.85</b>	<b>80.25</b>	<b>78.84</b>	<b>76.64</b>

Table 3: Temporal forgery localization results on AV-Deepfake1M [8]. Modality denotes the model’s input type with  $\mathcal{V}$  being visual and  $\mathcal{A}$  audio. **Bold** indicates best and underline second to best performance.

Method	Modality	AUC
F <sup>3</sup> -Net [55]	$\mathcal{V}$	52.0
MDS [14]	$\mathcal{AV}$	82.8
EfficientViT [17]	$\mathcal{V}$	96.5
BA-TFD [10]	$\mathcal{AV}$	99.0
UMMAFormer [76]	$\mathcal{AV}$	<b>99.8</b>
DiMoDif (ours)	$\mathcal{AV}$	<u>99.6</u>

Table 4: Deepfake detection results on LAV-DF [10]. Modality denotes the model’s input type with  $\mathcal{V}$  being visual and  $\mathcal{A}$  audio. **Bold** indicates best and underline second to best performance.

Method	Modality	AUC	ACC
Video-LLaMA (13B) E5 [75]	$\mathcal{AV}$	50.7	25.1
LipForensics [29]	$\mathcal{V}$	51.6	68.8
Face X-Ray [38]	$\mathcal{V}$	61.5	73.8
Meso4 [1]	$\mathcal{V}$	50.2	75.0
MesoInception4 [1]	$\mathcal{V}$	50.1	75.0
SBI [62]	$\mathcal{V}$	<u>65.8</u>	69.0
MDS [14]	$\mathcal{AV}$	56.6	59.4
DiMoDif (ours)	$\mathcal{AV}$	<b>96.3</b>	83.3*

Table 5: Deepfake detection results on AV-Deepfake1M [8]. Modality denotes the model’s input type with  $\mathcal{V}$  being visual and  $\mathcal{A}$  audio. **Bold** indicates best and underline second to best performance. \*Validation set accuracy is reported as Codabench only provides AUC score.

### 5.3 Generalization

This paper is the first to conduct generalization experiments on the used datasets. Table 7 presents DiMoDif’s cross-dataset performance on DFD. Training on FakeAVCeleb [34] leads to poor performance on LAV-DF, AV-Deepfake1M, and DFDC but to moderate performance on KoDF with 77.4 AP. Training on LAV-DF [10] leads to moderate performance on FakeAVCeleb and AV-Deepfake1M, low performance on DFDC but good performance on KoDF with 88.8 AP. Training on AV-Deepfake1M [8] dataset leads to high scores on FakeAVCeleb and LAV-DF with 85.4

AUC and 81.5 AUC respectively, moderate performance on KoDF with 77.7 AP, but low performance on DFDC. In general, low generalization is observed on DFDC, which can be partly explained by the discussion in Section 2.1. Our models focus on cross-modal information differences, while many DFDC videos do not contain talking or the talking person is different from the depicted one; thus, a visual-only face manipulation detector would likely lead to better results. Appendix C provides detailed generalization evaluation on FakeAVCeleb with scores per forgery type. Table 8 presents cross-dataset performance on TFL. Training on AV-Deepfake1M leads to acceptable performance

Method	Modality	Pre-training	Category												
			RVFA		FVRA-WL		FVFA-WL		FVFA-FS		FVFA-GAN		AVG-FV		
			AP	AUC	AP	AUC	AP	AUC	AP	AUC	AP	AUC	AP	AUC	
Unsupervised	AVBYOL [25]	$\mathcal{AV}$	LRW [16]	50.0	50.0	73.4	61.3	88.7	80.8	60.2	33.8	73.2	61.0	73.9	59.2
	VQ-GAN [21]	$\mathcal{V}$	LRS2 [2]	-	-	50.3	49.3	57.5	53.0	49.6	48.0	62.4	56.9	55.0	51.8
	AVAD [22]	$\mathcal{AV}$	LRS2 [2]	62.4	71.6	93.6	93.7	95.3	95.8	94.1	94.3	93.8	94.1	94.2	94.5
	AVAD [22]	$\mathcal{AV}$	LRS3 [3]	70.7	<u>80.5</u>	91.1	93.0	91.0	92.3	91.6	92.7	91.4	93.1	91.3	92.8
Supervised	Xception [58]	$\mathcal{V}$	ImageNet [19]	-	-	88.2	88.3	92.3	93.5	67.6	68.5	91.0	91.0	84.8	85.3
	LipForensics [29]	$\mathcal{V}$	LRW [16]	-	-	<u>97.8</u>	<u>97.7</u>	<u>99.9</u>	<u>99.9</u>	61.5	68.1	98.6	98.7	89.4	91.1
	AD DFD [80]	$\mathcal{AV}$	Kinetics [33]	<u>74.9</u>	73.3	97.0	97.4	99.6	99.7	58.4	55.4	<b>100.</b>	<b>100.</b>	88.8	88.1
	FTCN [78]	$\mathcal{V}$	-	-	-	96.2	97.4	<b>100.</b>	<b>100.</b>	77.4	78.3	95.6	96.5	92.3	93.1
	RealForensics [28]	$\mathcal{V}$	LRW [16]	-	-	88.8	93.0	99.3	99.1	<b>99.8</b>	<u>99.8</u>	93.4	96.7	<u>95.3</u>	<u>97.1</u>
	DiMoDif (ours)	$\mathcal{AV}$	-	-	<b>84.5</b>	<b>97.1</b>	<b>99.0</b>	<b>99.9</b>	99.7	<u>99.9</u>	<u>99.5</u>	<b>99.9</b>	<u>99.6</u>	<u>99.9</u>	<b>99.4</b>

Table 6: Deepfake detection results on FakeAVCeleb [34]. Modality denotes the model’s input type with  $\mathcal{V}$  being visual and  $\mathcal{A}$  audio. **Bold** indicates best and underline second to best performance. Supervised methods that use pre-training are fine-tuned on FakeAVCeleb, while unsupervised methods are not trained with labels and fake examples.

Training dataset	Test dataset	Test dataset														
		FakeAVCeleb [34]			LAV-DF [10]			AV-Deepfake1M [8]			DFDC [20]			KoDF [36]		
		ACC	AP	AUC	ACC	AP	AUC	ACC	AP	AUC	ACC	AP	AUC	ACC	AP	AUC
Training dataset	FakeAVCeleb [34]	98.1	99.9	99.9	39.3	59.5	61.9	25.3	55.1	55.1	51.4	62.7	60.8	65.5	77.4	32.7
	LAV-DF [10]	43.6	70.7	71.3	95.6	99.6	99.6	32.1	69.7	66.2	51.8	52.9	54.5	43.8	88.8	66.5
	AV-Deepfake1M [8]	56.3	82.0	85.4	59.2	83.2	81.5	87.7	97.3	97.3	51.3	50.5	49.7	77.0	77.7	33.4

Table 7: Generalization performance on Deepfake detection task.

Training dataset	Test dataset										
	AP@0.5	AP@0.75	AP@0.9	AP@0.95	AR@100	AR@50	AR@30	AR@20	AR@10	AR@5	
	Test dataset: LAV-DF										
Training dataset	LAV-DF [10]	95.5	87.9	54.6	20.6	94.2	93.7	93.2	92.7	91.4	89.2
	AV-Deepfake1M [8]	59.8	26.2	2.3	0.2	75.3	72.3	69.7	67.3	62.5	56.2
Test dataset: AV-Deepfake1M											
Training dataset	LAV-DF [10]	16.8	4.6	0.3	0.0	31.9	30.1	28.6	27.0	23.6	19.9
	AV-Deepfake1M [8]	96.0	86.2	34.5	6.9	89.2	88.7	88.2	87.7	86.4	84.3

Table 8: Generalization performance on Temporal Forgery Localization task.

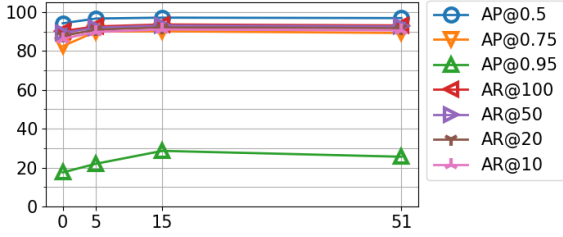
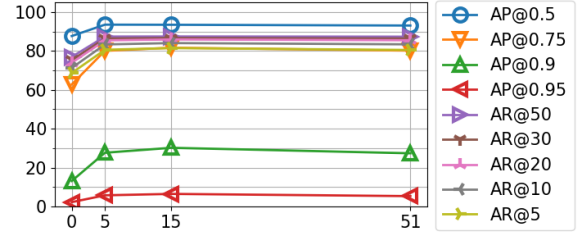
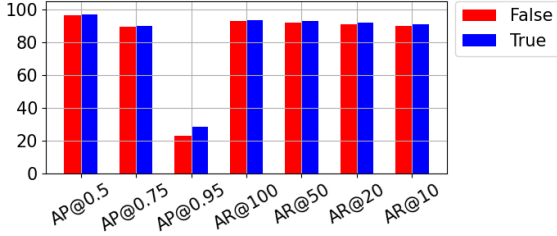
on LAV-DF, in contrast to training on LAV-DF and evaluating on AV-Deepfake1M. performance.

## 5.4 Ablation Analysis

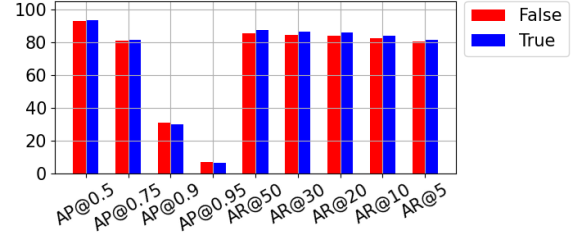
Figure 3 presents an ablation analysis that supports our methodological choices. For AV-Deepfake1M we report validation performance as conducting the ablations through Codabench would be impractical. These results pertain to TFL, while further ablations as well as the same analysis wrt DFD can be found in Appendix D. Figures 3a and 3b indicate that a small window size  $q = 15$  for Transformer’s  $\mathcal{T}$  local attention is optimal, especially in contrast to attending on all tokens determined by  $q = 0$ . Also, the feature pyramid scheme provides a small performance increase as indicated by Figures 3c and 3d. The size of  $\mathcal{T}$  plays crucial role in achieving maximum performance as shown in Figures 3e and 3f, both in terms of number of layers  $l$  and layer size determined by input dimension  $d$ , number of attention heads  $r$ , and internal dimension  $d \cdot u$ . Specifically, the larger the model the higher its

## 6 Conclusions

In this work, we propose an audio-visual deepfake detection and localization framework that leverages cross-modal differences in machine perception of speech. It hinges on the assumption that the visual and audio signals of videos with real discourse coincide wrt information, in contrast to deepfakes that exhibit cross-modal incongruities. It considers a video and audio speech recognition feature extraction stage, and a Transformer encoder-based learning stage along with a combination of three loss functions that optimize frame-level detection, predicted interval overlap, and boundaries. An extensive evaluation study indicates the effectiveness of our framework reaching state-of-the-art performance and in several cases surpassing it. Our model is limited by the languages recognized by the used speech-recognition backbones, although it exhibits good generalization to Korean. Also, it as-

(a) Window size  $q$  (LAV-DF)(b) Window size  $q$  (AV-Deepfake1M)

(c) Feature pyramid use (LAV-DF)



(d) Feature pyramid use (AV-Deepfake1M)

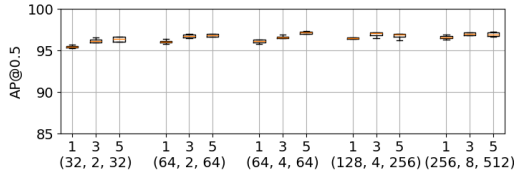
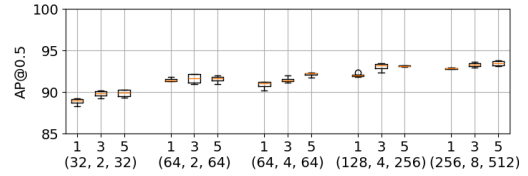
(e) Transformer  $\mathcal{T}$  size ( $d, r, d \cdot u$ ) (LAV-DF)(f) Transformer  $\mathcal{T}$  size ( $d, r, d \cdot u$ ) (AV-Deepfake1M)

Figure 3: Ablation and hyperparameter tuning analysis.

sumes one continually visible speaking person, at least moderate video quality and face size to detect face landmarks, and requires both modalities for manipulation detection. Future work includes joint training on Deepfake Detection and Temporal Forgery Localization tasks to assess potential benefits and extension to multiple speakers.

## 7 Acknowledgments

This work has been partially funded by the Horizon Europe projects A14Trust (GA No. 101070190) and vera.ai (GA No. 101070093).

## References

- [1] Darius Afchar, Vincent Nozick, Junichi Yamagishi, and Isao Echizen. Mesonet: a compact facial video forgery detection network. In *2018 IEEE international workshop on information forensics and security (WIFS)*, pages 1–7. IEEE, 2018. 3, 6
- [2] Triantafyllos Afouras, Joon Son Chung, Andrew Senior, Oriol Vinyals, and Andrew Zisserman. Deep audio-visual speech recognition. *IEEE transactions on pattern analysis and machine intelligence*, 44(12):8717–8727, 2018. 7
- [3] Triantafyllos Afouras, Joon Son Chung, and Andrew Zisserman. Lrs3-ted: a large-scale dataset for visual speech recognition. *arXiv preprint arXiv:1809.00496*, 2018. 7
- [4] Luc H Arnal, Valentin Wyart, and Anne-Lise Giraud. Transitions in neural oscillations reflect prediction errors generated in audiovisual speech. *Nature neuroscience*, 14(6):797–801, 2011. 1
- [5] Anurag Bagchi, Jazib Mahmood, Dolton Fernandes, and Ravi Kiran Sarvadevabhatla. Hear me out: Fusional approaches for audio augmented temporal action localization. *arXiv preprint arXiv:2106.14118*, 2021. 3, 6
- [6] Helen L Bear and Richard Harvey. Phoneme-to-viseme mappings: the good, the bad, and the ugly. *Speech Communication*, 95:40–67, 2017. 2
- [7] Matyas Bohacek and Hany Farid. Lost in translation: Lip-sync deepfake detection from audio-video mismatch. In *Proceedings of the IEEE/CVF Conference on Computer Vision and Pattern Recognition*, pages 4315–4323, 2024. 3
- [8] Zhixi Cai, Shreya Ghosh, Aman Pankaj Adatia, Munawar Hayat, Abhinav Dhalla, and Kalin Stefanov. Av-deepfake1m: A large-scale llm-driven audio-visual deepfake dataset. *arXiv preprint arXiv:2311.15308*, 2023. 2, 3, 5, 6, 7, 15



- [9] Zhixi Cai, Shreya Ghosh, Abhinav Dhall, Tom Gedeon, Kalin Stefanov, and Munawar Hayat. Glitch in the matrix: A large scale benchmark for content driven audio–visual forgery detection and localization. *Computer Vision and Image Understanding*, 236:103818, 2023. 1, 3, 5, 6
- [10] Zhixi Cai, Kalin Stefanov, Abhinav Dhall, and Munawar Hayat. Do you really mean that? content driven audio-visual deepfake dataset and multimodal method for temporal forgery localization. In *2022 International Conference on Digital Image Computing: Techniques and Applications (DICTA)*, pages 1–10. IEEE, 2022. 2, 3, 5, 6, 7, 15
- [11] Junyi Cao, Chao Ma, Taiping Yao, Shen Chen, Shouhong Ding, and Xiaokang Yang. End-to-end reconstruction-classification learning for face forgery detection. In *Proceedings of the IEEE/CVF Conference on Computer Vision and Pattern Recognition*, pages 4113–4122, 2022. 1
- [12] C. Chandrasekaran and A. Ghazanfar. When what you see is not what you hear. *Nature Neuroscience*, 14:675–676, 2011. 1
- [13] Lihan Chen, Xiaolin Zhou, Hermann J Müller, and Zhuanghua Shi. What you see depends on what you hear: Temporal averaging and cross-modal integration. *Journal of Experimental Psychology: General*, 147(12):1851, 2018. 1
- [14] Komal Chugh, Parul Gupta, Abhinav Dhall, and Ramanathan Subramanian. Not made for each other-audio-visual dissonance-based deepfake detection and localization. In *Proceedings of the 28th ACM international conference on multimedia*, pages 439–447, 2020. 1, 3, 6
- [15] Joon Son Chung, Arsha Nagrani, and Andrew Senior. Voxceleb2: Deep speaker recognition. *arXiv preprint arXiv:1806.05622*, 2018. 3, 5
- [16] Joon Son Chung and Andrew Senior. Lip reading in the wild. In *Computer Vision—ACCV 2016: 13th Asian Conference on Computer Vision, Taipei, Taiwan, November 20–24, 2016, Revised Selected Papers, Part II 13*, pages 87–103. Springer, 2017. 7
- [17] Davide Alessandro Coccomini, Nicola Messina, Claudio Gennaro, and Fabrizio Falchi. Combining efficientnet and vision transformers for video deepfake detection. In *International conference on image analysis and processing*, pages 219–229. Springer, 2022. 3, 6
- [18] Davide Cozzolino, Alessandro Pianese, Matthias Nießner, and Luisa Verdoliva. Audio-visual person-of-interest deepfake detection. In *Proceedings of the IEEE/CVF conference on computer vision and pattern recognition*, pages 943–952, 2023. 1, 3
- [19] Jia Deng, Wei Dong, Richard Socher, Li-Jia Li, Kai Li, and Li Fei-Fei. Imagenet: A large-scale hierarchical image database. In *2009 IEEE conference on computer vision and pattern recognition*, pages 248–255. Ieee, 2009. 7
- [20] Brian Dolhansky, Joanna Bitton, Ben Pflaum, Jikuo Lu, Russ Howes, Menglin Wang, and Cristian Canton Ferrer. The deepfake detection challenge (dfdc) dataset. *arXiv preprint arXiv:2006.07397*, 2020. 3, 5, 7
- [21] Patrick Esser, Robin Rombach, and Bjorn Ommer. Taming transformers for high-resolution image synthesis. In *Proceedings of the IEEE/CVF conference on computer vision and pattern recognition*, pages 12873–12883, 2021. 3, 7
- [22] Chao Feng, Ziyang Chen, and Andrew Owens. Self-supervised video forensics by audio-visual anomaly detection. In *Proceedings of the IEEE/CVF Conference on Computer Vision and Pattern Recognition*, pages 10491–10503, 2023. 3, 7
- [23] Ross Girshick. Fast r-cnn. In *Proceedings of the IEEE international conference on computer vision*, pages 1440–1448, 2015. 5, 13
- [24] Irving John Good. Rational decisions. *Journal of the Royal Statistical Society: Series B (Methodological)*, 14(1):107–114, 1952. 4, 13
- [25] Jean-Bastien Grill, Florian Strub, Florent Altché, Corentin Tallec, Pierre Richemond, Elena Buchatskaya, Carl Doersch, Bernardo Avila Pires, Zhaohan Guo, Mohammad Gheshlaghi Azar, et al. Bootstrap your own latent—a new approach to self-supervised learning. *Advances in neural information processing systems*, 33:21271–21284, 2020. 3, 7
- [26] Yewei Gu, Xianfeng Zhao, Chen Gong, and Xiaowei Yi. Deepfake video detection using audio-visual consistency. In *Digital Forensics and Watermarking: 19th International Workshop, IWDW 2020, Melbourne, VIC, Australia, November 25–27, 2020, Revised Selected Papers 19*, pages 168–180. Springer, 2021. 1, 3
- [27] Zhihao Gu, Yang Chen, Taiping Yao, Shouhong Ding, Jilin Li, and Lizhuang Ma. Delving into the local: Dynamic inconsistency learning for deepfake video detection. In *Proceedings of the AAAI Conference on Artificial Intelligence*, volume 36, pages 744–752, 2022. 1
- [28] Alexandros Haliassos, Rodrigo Mira, Stavros Petridis, and Maja Pantic. Leveraging real talking faces via self-supervision for robust forgery detection. In *Proceedings of the IEEE/CVF Conference on Computer Vision and Pattern Recognition*, pages 14950–14962, 2022. 1, 3, 7

- [29] Alexandros Haliassos, Konstantinos Vougioukas, Stavros Petridis, and Maja Pantic. Lips don't lie: A generalisable and robust approach to face forgery detection. In *Proceedings of the IEEE/CVF conference on computer vision and pattern recognition*, pages 5039–5049, 2021. [3](#), [6](#), [7](#)
- [30] Peisong He, Haoliang Li, and Hongxia Wang. Detection of fake images via the ensemble of deep representations from multi color spaces. In *2019 IEEE international conference on image processing (ICIP)*, pages 2299–2303. IEEE, 2019. [1](#)
- [31] Hafsa Ilyas, Ali Javed, and Khalid Mahmood Malik. Avfakenet: A unified end-to-end dense swin transformer deep learning model for audio-visual deepfakes detection. *Applied Soft Computing*, 136:110124, 2023. [3](#)
- [32] Liming Jiang, Ren Li, Wayne Wu, Chen Qian, and Chen Change Loy. Deeperforensics-1.0: A large-scale dataset for real-world face forgery detection. In *Proceedings of the IEEE/CVF conference on computer vision and pattern recognition*, pages 2889–2898, 2020. [3](#)
- [33] Will Kay, Joao Carreira, Karen Simonyan, Brian Zhang, Chloe Hillier, Sudheendra Vijayanarasimhan, Fabio Viola, Tim Green, Trevor Back, Paul Natsev, et al. The kinetics human action video dataset. *arXiv preprint arXiv:1705.06950*, 2017. [7](#)
- [34] Hasam Khalid, Shahroz Tariq, Minha Kim, and Simon S Woo. Fakeavceleb: A novel audio-video multimodal deepfake dataset. *arXiv preprint arXiv:2108.05080*, 2021. [2](#), [3](#), [5](#), [6](#), [7](#), [13](#), [15](#)
- [35] Pavel Korshunov and Sébastien Marcel. Deepfakes: a new threat to face recognition? assessment and detection. *arXiv preprint arXiv:1812.08685*, 2018. [3](#)
- [36] Patrick Kwon, Jaeseong You, Gyuhyeon Nam, Sungwoo Park, and Gyeongsu Chae. Kodf: A large-scale korean deepfake detection dataset. In *Proceedings of the IEEE/CVF international conference on computer vision*, pages 10744–10753, 2021. [3](#), [5](#), [7](#)
- [37] Jimmy Lei Ba, Jamie Ryan Kiros, and Geoffrey E Hinton. Layer normalization. *ArXiv e-prints*, pages arXiv-1607, 2016. [4](#)
- [38] Lingzhi Li, Jianmin Bao, Ting Zhang, Hao Yang, Dong Chen, Fang Wen, and Baining Guo. Face x-ray for more general face forgery detection. In *Proceedings of the IEEE/CVF conference on computer vision and pattern recognition*, pages 5001–5010, 2020. [3](#), [6](#)
- [39] Xiaolou Li, Zehua Liu, Chen Chen, Lantian Li, Li Guo, and Dong Wang. Zero-shot fake video detection by audio-visual consistency. In *Inter-speech 2024*, pages 2935–2939, 2024. [3](#)
- [40] Yuezun Li, Ming-Ching Chang, and Siwei Lyu. In ictu oculi: Exposing ai created fake videos by detecting eye blinking. In *2018 IEEE International workshop on information forensics and security (WIFS)*, pages 1–7. Ieee, 2018. [1](#)
- [41] Yuezun Li, Xin Yang, Pu Sun, Honggang Qi, and Siwei Lyu. Celeb-df: A large-scale challenging dataset for deepfake forensics. In *Proceedings of the IEEE/CVF conference on computer vision and pattern recognition*, pages 3207–3216, 2020. [3](#)
- [42] Tianwei Lin, Xiao Liu, Xin Li, Errui Ding, and Shilei Wen. Bmn: Boundary-matching network for temporal action proposal generation. In *Proceedings of the IEEE/CVF international conference on computer vision*, pages 3889–3898, 2019. [3](#), [6](#)
- [43] Tsung-Yi Lin, Priya Goyal, Ross Girshick, Kaiming He, and Piotr Dollár. Focal loss for dense object detection. In *Proceedings of the IEEE international conference on computer vision*, pages 2980–2988, 2017. [5](#), [13](#)
- [44] Pingchuan Ma, Stavros Petridis, and Maja Pantic. Visual speech recognition for multiple languages in the wild. *Nature Machine Intelligence*, 4(11):930–939, 2022. [1](#), [2](#), [4](#)
- [45] Momina Masood, Mariam Nawaz, Khalid Mahmood Malik, Ali Javed, Aun Irtaza, and Hafiz Malik. Deepfakes generation and detection: State-of-the-art, open challenges, countermeasures, and way forward. *Applied intelligence*, 53(4):3974–4026, 2023. [1](#)
- [46] Yisroel Mirsky and Wenke Lee. The creation and detection of deepfakes: A survey. *ACM computing surveys (CSUR)*, 54(1):1–41, 2021. [1](#)
- [47] Trisha Mittal, Uttaran Bhattacharya, Rohan Chandra, Aniket Bera, and Dinesh Manocha. Emotions don't lie: An audio-visual deepfake detection method using affective cues. In *Proceedings of the 28th ACM international conference on multimedia*, pages 2823–2832, 2020. [3](#)
- [48] Kartik Narayan, Harsh Agarwal, Kartik Thakral, Surbhi Mittal, Mayank Vatsa, and Richa Singh. Df-platter: Multi-face heterogeneous deepfake dataset. In *Proceedings of the IEEE/CVF Conference on Computer Vision and Pattern Recognition*, pages 9739–9748, 2023. [3](#)
- [49] Audrey R Nath and Michael S Beauchamp. A neural basis for interindividual differences in the mcgurk effect, a multisensory speech illusion. *Neuroimage*, 59(1):781–787, 2012. [1](#)

- [50] Megha Nawhal and Greg Mori. Activity graph transformer for temporal action localization. *arXiv preprint arXiv:2101.08540*, 2021. **3, 6**
- [51] Thanh Thi Nguyen, Quoc Viet Hung Nguyen, Dung Tien Nguyen, Duc Thanh Nguyen, Thien Huynh-The, Saeid Nahavandi, Thanh Tam Nguyen, Quoc-Viet Pham, and Cuong M Nguyen. Deep learning for deepfakes creation and detection: A survey. *Computer Vision and Image Understanding*, 223:103525, 2022. **1**
- [52] Casey O’Callaghan. Seeing what you hear: Cross-modal illusions and perception. *Philosophical Issues*, 18:316–338, 2008. **1**
- [53] Trevine Oorloff, Surya Koppiseti, Nicolò Bonetini, Divyaraj Solanki, Ben Colman, Yaser Yacoob, Ali Shahriyari, and Gaurav Bharaj. Avff: Audio-visual feature fusion for video deepfake detection. In *Proceedings of the IEEE/CVF Conference on Computer Vision and Pattern Recognition*, pages 27102–27112, 2024. **3**
- [54] Gan Pei, Jiangning Zhang, Menghan Hu, Guangtao Zhai, Chengjie Wang, Zhenyu Zhang, Jian Yang, Chunhua Shen, and Dacheng Tao. Deepfake generation and detection: A benchmark and survey. *arXiv preprint arXiv:2403.17881*, 2024. **1**
- [55] Yuyang Qian, Guojun Yin, Lu Sheng, Zixuan Chen, and Jing Shao. Thinking in frequency: Face forgery detection by mining frequency-aware clues. In *European conference on computer vision*, pages 86–103. Springer, 2020. **3, 6**
- [56] Muhammad Anas Raza and Khalid Mahmood Malik. Multimodaltrace: Deepfake detection using audiovisual representation learning. In *Proceedings of the IEEE/CVF Conference on Computer Vision and Pattern Recognition*, pages 993–1000, 2023. **3**
- [57] Tal Reiss, Bar Cavia, and Yedid Hoshen. Detecting deepfakes without seeing any. *arXiv preprint arXiv:2311.01458*, 2023. **3**
- [58] Andreas Rossler, Davide Cozzolino, Luisa Verdoliva, Christian Riess, Justus Thies, and Matthias Nießner. Faceforensics++: Learning to detect manipulated facial images. In *Proceedings of the IEEE/CVF international conference on computer vision*, pages 1–11, 2019. **3, 7**
- [59] Sahibzada Adil Shahzad, Ammarah Hashmi, Sarwar Khan, Yan-Tsung Peng, Yu Tsao, and Hsin-Min Wang. Lip sync matters: A novel multimodal forgery detector. In *2022 Asia-Pacific Signal and Information Processing Association Annual Summit and Conference (APSIPA ASC)*, pages 1885–1892. IEEE, 2022. **3**
- [60] Ladan Shams, Yukiyasu Kamitani, and Shinsuke Shimojo. Visual illusion induced by sound. *Cognitive brain research*, 14(1):147–152, 2002. **1**
- [61] Dingfeng Shi, Yujie Zhong, Qiong Cao, Lin Ma, Jia Li, and Dacheng Tao. Tridet: Temporal action detection with relative boundary modeling. In *Proceedings of the IEEE/CVF Conference on Computer Vision and Pattern Recognition*, pages 18857–18866, 2023. **3, 6**
- [62] Kaede Shiohara and Toshihiko Yamasaki. Detecting deepfakes with self-blended images. In *Proceedings of the IEEE/CVF Conference on Computer Vision and Pattern Recognition*, pages 18720–18729, 2022. **3, 6**
- [63] Paula C Stacey, Pádraig T Kitterick, Saffron D Morris, and Christian J Sumner. The contribution of visual information to the perception of speech in noise with and without informative temporal fine structure. *Hearing research*, 336:17–28, 2016. **1**
- [64] William H Sumby and Irwin Pollack. Visual contribution to speech intelligibility in noise. *The journal of the acoustical society of america*, 26(2):212–215, 1954. **1**
- [65] Chuangchuang Tan, Yao Zhao, Shikui Wei, Guanghua Gu, and Yunchao Wei. Learning on gradients: Generalized artifacts representation for gan-generated images detection. In *Proceedings of the IEEE/CVF Conference on Computer Vision and Pattern Recognition*, pages 12105–12114, 2023. **1**
- [66] A Vaswani. Attention is all you need. *Advances in Neural Information Processing Systems*, 2017. **2, 4**
- [67] Limin Wang, Bingkun Huang, Zhiyu Zhao, Zhan Tong, Yinan He, Yi Wang, Yali Wang, and Yu Qiao. Videomae v2: Scaling video masked autoencoders with dual masking. In *Proceedings of the IEEE/CVF Conference on Computer Vision and Pattern Recognition*, pages 14549–14560, 2023. **6**
- [68] Yi Wang, Kunchang Li, Yizhuo Li, Yinan He, Bingkun Huang, Zhiyu Zhao, Hongjie Zhang, Jilan Xu, Yi Liu, Zun Wang, et al. Internvideo: General video foundation models via generative and discriminative learning. *arXiv preprint arXiv:2212.03191*, 2022. **6**
- [69] Yujia Wang and Hua Huang. Audio-visual deepfake detection using articulatory representation learning. *Computer Vision and Image Understanding*, page 104133, 2024. **3**
- [70] Jamal R Williams, Yuri A Markov, Natalia A Tiurina, and Viola S Störmer. What you see is what you hear: sounds alter the contents of visual perception. *Psychological science*, 33(12):2109–2122, 2022. **1**

- [71] Wenyuan Yang, Xiaoyu Zhou, Zhikai Chen, Bofei Guo, Zhongjie Ba, Zhihua Xia, Xiaochun Cao, and Kui Ren. Avoid-df: Audio-visual joint learning for detecting deepfake. *IEEE Transactions on Information Forensics and Security*, 18:2015–2029, 2023. [3](#)
- [72] Xin Yang, Yuezun Li, and Siwei Lyu. Exposing deep fakes using inconsistent head poses. In *ICASSP 2019-2019 IEEE International Conference on Acoustics, Speech and Signal Processing (ICASSP)*, pages 8261–8265. IEEE, 2019. [1](#)
- [73] Yang Yu, Xiaolong Liu, Rongrong Ni, Siyuan Yang, Yao Zhao, and Alex C Kot. Pvass-mdd: predictive visual-audio alignment self-supervision for multimodal deepfake detection. *IEEE Transactions on Circuits and Systems for Video Technology*, 2023. [3](#)
- [74] Chen-Lin Zhang, Jianxin Wu, and Yin Li. Actionformer: Localizing moments of actions with transformers. In *European Conference on Computer Vision*, pages 492–510. Springer, 2022. [3](#), [5](#), [6](#)
- [75] Hang Zhang, Xin Li, and Lidong Bing. Videollama: An instruction-tuned audio-visual language model for video understanding. *arXiv preprint arXiv:2306.02858*, 2023. [3](#), [6](#)
- [76] Rui Zhang, Hongxia Wang, Mingshan Du, Hanqing Liu, Yang Zhou, and Qiang Zeng. Ummaformer: A universal multimodal-adaptive transformer framework for temporal forgery localization. In *Proceedings of the 31st ACM International Conference on Multimedia*, pages 8749–8759, 2023. [1](#), [3](#), [5](#), [6](#)
- [77] Yibo Zhang, Weiguo Lin, and Junfeng Xu. Joint audio-visual attention with contrastive learning for more general deepfake detection. *ACM Transactions on Multimedia Computing, Communications and Applications*, 20(5):1–23, 2024. [3](#)
- [78] Yinglin Zheng, Jianmin Bao, Dong Chen, Ming Zeng, and Fang Wen. Exploring temporal coherence for more general video face forgery detection. In *Proceedings of the IEEE/CVF international conference on computer vision*, pages 15044–15054, 2021. [3](#), [7](#)
- [79] Zhaohui Zheng, Ping Wang, Wei Liu, Jinze Li, Rongguang Ye, and Dongwei Ren. Distance-iou loss: Faster and better learning for bounding box regression. In *Proceedings of the AAAI conference on artificial intelligence*, volume 34, pages 12993–13000, 2020. [5](#), [13](#)
- [80] Yipin Zhou and Ser-Nam Lim. Joint audio-visual deepfake detection. In *Proceedings of the IEEE/CVF International Conference on Computer Vision*, pages 14800–14809, 2021. [3](#), [7](#)
- [81] Bojia Zi, Minghao Chang, Jingjing Chen, Xingjun Ma, and Yu-Gang Jiang. Wilddeepfake: A challenging real-world dataset for deepfake detection. In *Proceedings of the 28th ACM international conference on multimedia*, pages 2382–2390, 2020. [3](#)
- [82] Heqing Zou, Meng Shen, Yuchen Hu, Chen Chen, Eng Siong Chng, and Deepu Rajan. Cross-modality and within-modality regularization for audio-visual deepfake detection. In *ICASSP 2024-2024 IEEE International Conference on Acoustics, Speech and Signal Processing (ICASSP)*, pages 4900–4904. IEEE, 2024. [3](#)

## A Objective function details

For the DFD task, we consider the binary cross-entropy loss [24], directly optimizing the real vs. fake objective:

$$\mathcal{L}_{DFD} = -\frac{1}{2l} \sum_{m \in \{v,a\}} \sum_{j=1}^l y[m] \log \hat{y}[j, m] + (1 - y[m]) \cdot \log(1 - \hat{y}[j, m]) \quad (7)$$

where  $j$  is layer index,  $m$  is modality index, and  $x[\cdot]$  is used to denote vector or matrix element access operation (array indexing).

For the TFL task, we consider a combination of three loss functions. For clarity we omit to also include the symbols for the averaging across  $l$  layers, which however takes place as well. Specifically, we use:

1. The focal loss [43] to optimize the classification objective, while accounting for class imbalance being prevalent among each video’s frames:

$$\mathcal{L}_{focal} = \sum_{m \in \{v,a\}} \sum_{j=1}^f -\alpha_t^{m,j} (1 - p_t^{m,j})^\gamma \log(p_t^{m,j}) \quad (8)$$

in which:

$$\alpha_t^{m,j} = \begin{cases} \alpha & \text{if } y_j^m = 1 \\ 1 - \alpha & \text{otherwise} \end{cases} \quad (9)$$

$$p_t^{m,j} = \begin{cases} \hat{y}_j^m & \text{if } y_j^m = 1 \\ 1 - \hat{y}_j^m & \text{otherwise} \end{cases} \quad (10)$$

while  $\alpha$  and  $\gamma$  are hyperparameters.

2. The DIoU loss [79] to optimize the regression objective by maximizing the overlap between predicted and ground truth fake time intervals:

$$\mathcal{L}_{DIoU} = \sum_{m \in \{v,a\}} \sum_{j=1}^f \left( 1.0 - \text{IoU}(\hat{\mathbf{b}}_j^m, \mathbf{b}_j^m) + \frac{\rho^2(\hat{b}_j^m, b_j^m)}{\kappa^2} \right) \cdot \mathbb{1}_{m,j} \quad (11)$$

where  $j$  is frame index,  $m$  is modality index, IoU denotes intersection over union,  $\mathbf{b}_j^m = [s_j^m, e_j^m]$  denotes a time interval,  $b_j^m = 0.5 \cdot (e_j^m + s_j^m)$  denotes the interval’s center,  $\rho$  denotes the Euclidean distance,  $\kappa$  denotes the length of the smallest enclosing interval covering both predicted and ground truth intervals, and  $\mathbb{1}_{m,j}$  is an indicator function that denotes if frame  $j$  of modality  $m$  is fake.

3. The smooth L1 loss [23] to minimize the distance between predicted and actual boundaries of fake time intervals:

$$\mathcal{L}_1^{smooth} = \sum_{m \in \{v,a\}} \sum_{j=1}^f \frac{1}{2} \left( h(s_j^m - \hat{s}_j^m) + h(e_j^m - \hat{e}_j^m) \right) \cdot \mathbb{1}_{m,j} \quad (12)$$

in which  $\mathbb{1}_{m,j}$  is an indicator function that denotes if frame  $j$  of modality  $m$  is fake, and  $h$  is defined as:

$$h(x) = \begin{cases} 0.5x^2 & \text{if } |x| < 1 \\ |x| - 0.5 & \text{otherwise} \end{cases} \quad (13)$$

We combine the three loss functions with addition divided by the total number of fake visual and audio frames  $p = \sum_{m \in \{v,a\}} \sum_{j=1}^f \mathbb{1}_{m,j}$ :

$$\mathcal{L}_{TFL} = (\mathcal{L}_{focal} + \mathcal{L}_{DIoU} + \mathcal{L}_1^{smooth}) / p \quad (14)$$

We finally average both  $\mathcal{L}_{DFD}$  and  $\mathcal{L}_{TFL}$  across batch samples during training.

## B Dataset class and split sizes

Table 9 provides details on dataset class and split sizes. Although, FakeAVCeleb paper [34] reports 10,000 FVFA and 9,000 FVRA samples, the download from the corresponding homepage <https://sites.google.com/view/fakeavcelebdash-lab> contains 10,835 and 9,709 respectively, resulting in 21.5K total number of samples instead of the commonly reported 20,000 size for this dataset. Documentation therein also claims “Since we apply the manual screening process on synthesized videos, the final video count is more than 20,000.”. Test metadata of AV-Deepfake1M have not been released but evaluation is enabled through Codabench.

## C Generalization on FakeAVCeleb

Table 10 provides a more detailed generalization evaluation on the FakeAVCeleb dataset with scores per forgery type, indicating the effectiveness of training on AV-Deepfake1M especially in some cases such as FVFA-WL and FVFA-FS reaching 95.6 AUC and 94.5 AUC, respectively. Training on LAV-DF also results in good generalization especially in FVFA-FS case with 90.0 AUC.

## D Ablation Analysis (further experiments)

Figures 4a and 4b indicate little to no sensitivity to the focal loss’ hyperparameter  $\alpha$ . Figures 4c and 4d indicate that the use of a learning rate scheduler is beneficial however the type of scheduler is not significantly affecting the results. Figure 5 indicates that on DFD window size  $q = 15$  is again optimal, but performance is not increased with feature pyramids nor with different learning rate schedules. Also, medium-sized models achieve maximum performance.

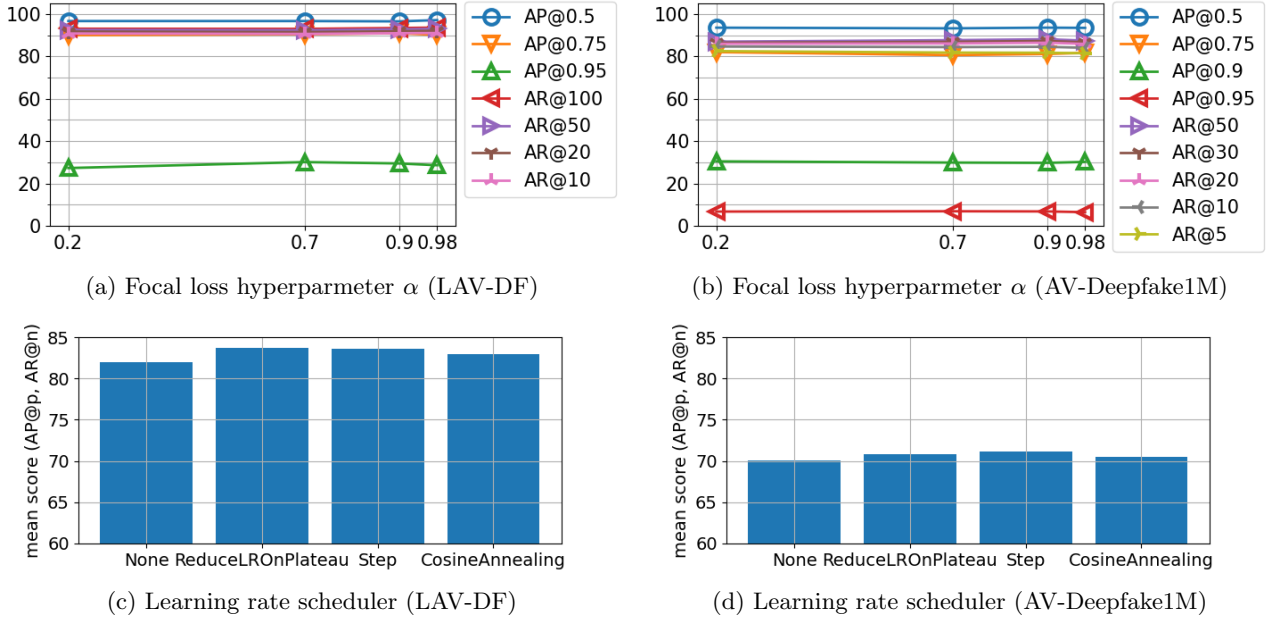


Figure 4: Ablation analysis on Temporal Forgery Localization task.

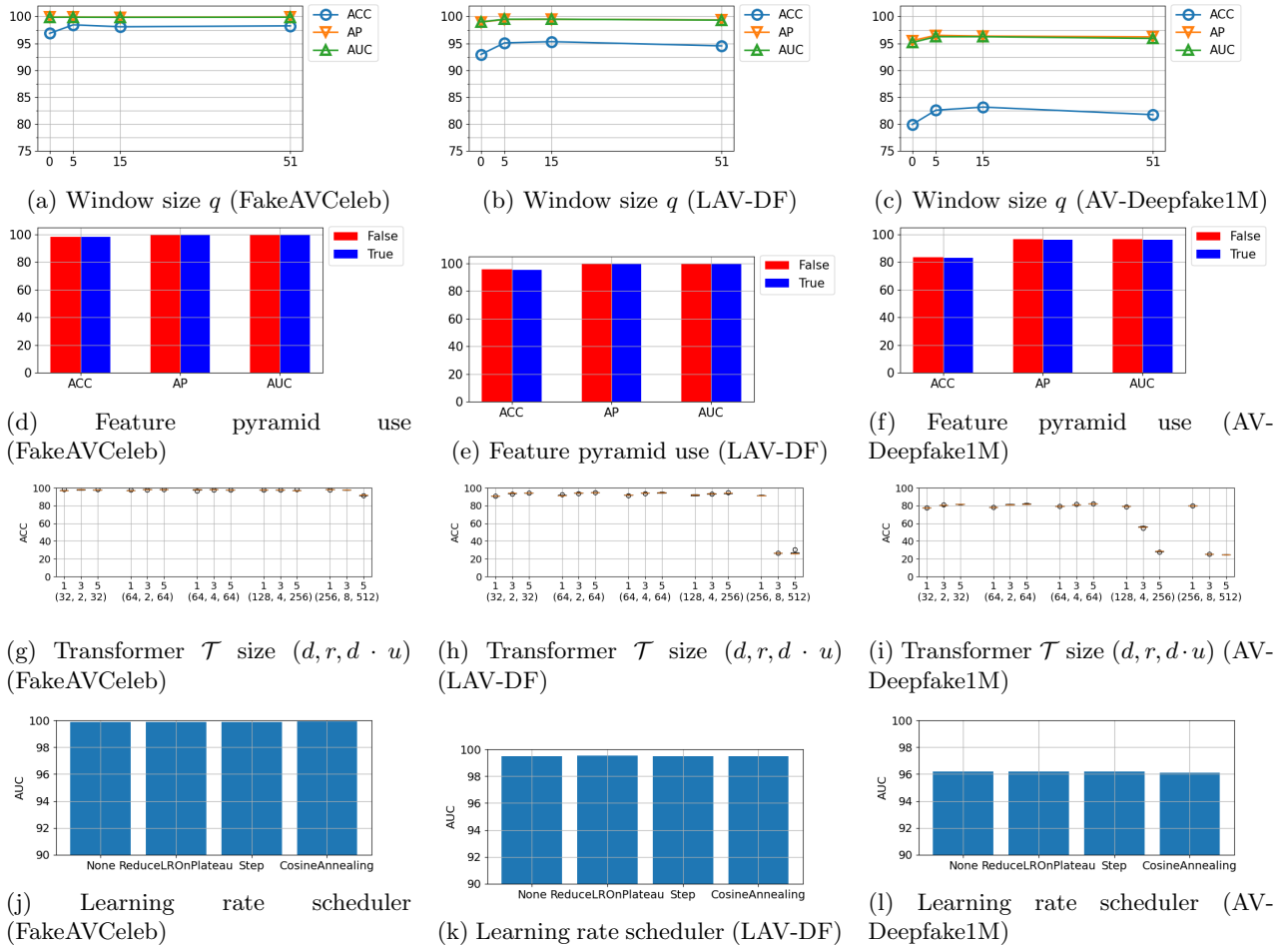


Figure 5: Ablation and hyperparameter tuning analysis on Deepfake Detection task.

	FakeAVCeleb				LAV-DF				AV-Deepfake1M			
	train	val	test	total	train	val	test	total	train	val	test	total
FVFA	8,678	1,052	1,105	10,835	19,090	7,701	6,369	33,160	186,344	14,515	-	-
FVRA	7,760	975	974	9,709	19,271	7,820	6,452	33,543	186,597	14,304	-	-
RVFA	399	49	52	500	19,088	7,709	6,373	33,170	186,573	14,286	-	-
RVRA	17,766	1,535	1,199	20,500	21,254	8,271	6,906	36,431	186,666	14,235	-	-
total	34,603	3,611	3,330	41,544	78,703	31,501	26,100	136,304	746,180	57,340	343,240	1,146,760

Table 9: Dataset class and split sizes. F: fake, R: real, V: video, A: audio.

Training dataset	Category											
	RVFA		FVRA-WL		FVFA-WL		FVFA-FS		FVFA-GAN		AVG-FV	
	AP	AUC	AP	AUC	AP	AUC	AP	AUC	AP	AUC	AP	AUC
FakeAVCeleb [34]	84.5	97.1	99.0	99.9	99.7	99.9	99.5	99.9	99.6	99.9	99.4	99.9
LAV-DF [10]	40.2	74.3	77.1	87.2	78.2	87.8	72.1	90.0	70.0	86.9	74.4	88.0
AV-Deepfake1M [8]	18.8	80.8	63.5	80.3	85.6	95.6	74.2	94.5	75.9	93.8	74.8	91.1

Table 10: Detailed generalization performance for each forgery type of the FakeAVCeleb dataset.